Active Suspension Control With Direct-Drive Tubular Linear Brushless Permanent-Magnet Motor

Seungho Lee, *Student Member, IEEE*, and Won-jong Kim, *Senior Member, IEEE*

***Abstract*—Recently, active suspension is gaining popularity in commercial automobiles. To develop the control methodologies for active suspension control, a quarter-car test bed was built employing a direct-drive tubular linear brushless permanent-magnet motor (LBPMM) as a force-generating component. Two accelerometers and a linear variable differential transformer (LVDT) are used in this quarter-car test bed. Three pulse-width-modulation (PWM) amplifiers supply the currents in three phases. Simulated road disturbance is generated by a rotating cam. Modified lead-lag control, linear-quadratic (LQ) servo control with a Kalman filter, fuzzy control methodologies were implemented for active-suspension control. In the case of fuzzy control, an asymmetric membership function was introduced to eliminate the DC offset in sensor data and to reduce the discrepancy in the models. This controller could attenuate road disturbance by up to 77% in the sprung mass velocity and 69% in acceleration. The velocity and the acceleration data of the sprung mass are presented to compare the controllers' performance in the ride comfort of a vehicle. Both simulation and experimental results are presented to demonstrate the effectiveness of these control methodologies.**

***Index Terms*—Asymmetric membership function, fuzzy control, lead-lag control, LQ servo, quarter car, tubular linear actuator.**

I. Introduction

ACTIVE suspension supports a vehicle and isolates its passengers from road disturbances for ride quality and vehicle handling using force-generating components under feedback control. Notwithstanding its complexity, high cost, and power requirements, active suspension has been used by the luxury car manufacturers such as BMW, Mercedes-Benz, and Volvo. Development of an active-suspension system should be accompanied by the methodologies to control it. Considering costly commercial vehicles with active suspension, Allen constructed a quarter-car test bed to develop the control strategies [1].

Many researchers developed active-suspension control techniques [2]–[21]. These research results can be categorized according to the applied control theories. When it comes to the LQ control, Peng, *et al.* presented the virtual input signal determined by the LQ optimal theory for active-suspension control [2]. Tang and Zhang applied linear-quadratic-Gaussian (LQG) control, neural networks, and genetic algorithms in an active suspension and presented simulation results [3]. Sam, *et al.* applied LQ control to simulate an active-suspension system [4]. As for the robust control, Lauwerys, *et al.* developed a linear robust controller based on the μ-synthesis for the active suspension of a quarter car [5]. Wang, *et al.* presented the algorithm to reduce the order of the H_∞ controller in the application of active suspension [6]. They were able to reduce the controller's order by nearly one third while the performance was only slightly degraded. Concha and Cipriano developed a novel controller combined with the fuzzy and LQR controllers [7]. Gobbi, *et al.* proposed a new control method based on a stochastic optimization theory assuming that the road irregularity is a Gaussian random process and modeled an exponential power spectral density [8].

Savaresi, *et al.* developed a novel control strategy, called Acceleration-Driven-Damper (ADD) in semi-active suspensions. They minimized the vertical sprung mass acceleration by applying an optimal control algorithm [9]. Then Savaresi and Spelta had ADD compared to sky-hook (SH) damping [10]. Recently, they proposed an innovative algorithm that satisfies quasi-optimal performance based on an SH-ADD control algorithm [11]. Abbas, *et al.* applied sliding-mode control for nonlinear full-vehicle active suspension [12]. They considered not only the dynamics of the nonlinear full-vehicle active-suspension system but also the dynamics of the four actuators. Many neural-network controllers were also applied to active suspension. Jin, *et al.* developed a novel neural control strategy for an active suspension system [13]. By combining the integrated error approach with the traditional neural control, they were able to develop a simple-structure neural controller with small computational requirements, beneficial to real-time control. Kou and Fang established active suspension with an electro-hydrostatic actuator (EHA) and implemented a fuzzy controller [14]. They could attenuate the suspension deflection by 26.76% compared with passive suspension. Alleyne and Hedrick developed a nonlinear adaptive controller for active suspension with an electro-hydraulic actuator [15]. They analyzed a standard parameter adaptation scheme based on the Lyapunov analysis and presented a modified adaptation scheme for active suspension.

Several researchers used electro-hydraulic actuators for active suspension [14], [15]. Electro-hydraulic actuators are powerful and less bulky compared to conventional DC and AC actuators. Moreover, they can provide the sky-hook damping effect, an ideal design of suspension [16]. However, electro-hydraulic actuators are highly nonlinear because of their hydraulic components such as a servo-valve. In most studies, it was assumed that the chamber volume of the hydraulic actuator was

Manuscript received October 02, 2008; revised January 28, 2009; accepted July 30, 2009. Manuscript received in final form August 10, 2009. First published October 13, 2009; current version published June 23, 2010. Recommended by Associate Editor S. Devasia.

The authors are with Department of Mechanical Engineering, Texas A&M University, College Station, TX 77843 USA (e-mail: wckorealsh@neo.tamu.edu; wjkim@tamu.edu).

Color versions of one or more of the figures in this paper are available online at http://ieeexplore.ieee.org.

Digital Object Identifier 10.1109/TCST.2009.2030413

constant while in fact the volume varied with the piston motion. This introduced an additional uncertainty to the model. However, due to the compact design, an LBPMM like the one presented in Section II of this paper has less modeling uncertainty and nonlinearity. Moreover, this LBPMM is directly applicable to active suspension without converting rotary motion to linear motion [17]. Besides its smooth, precise translational motion without cogging, the fact that the length of the mover can be conveniently adjusted makes it one of the best candidates for the force-generating component in an active-suspension system. Other actuators such as an oleo-pneumatic unit [18] and a 3-degree-of-freedom (3-DOF) vibration-isolation system [19] were also used for active suspension. The drawbacks of these actuators are bulkiness and design complexity. The oleo-pneumatic unit required a sealing structure. The 3-DOF vibration-isolation system consisted of five tables, magnets, springs, dampers, which led to a large size.

Realistic models of the car were considered in several research projects. Gao, *et al.* proposed a load-dependent controller for active suspension control [20]. They considered the sprung mass of the car varied with the load condition and assumed this value was measurable online. With this information they developed a much less conservative controller compared to a previous robust-control approach. Yagiz, *et al.* considered not only vertical but also pitch and roll motions of a nonlinear 7-DOF vehicle model [21]. They developed a sliding-mode controller for the active suspension control in a full vehicle.

There are issues related with the limitations of active-suspension solutions. For example, Suda and Shiba proposed the energy-regeneration in active suspension to solve the energy problem [22]. They proposed an energy regenerative damper system that converts vibration energy into useful energy. Then the converted energy is used for active suspension.

Since a human body is most susceptible to vibration at around 3 Hz (20 rad/s) [23], disturbance from the road is modeled as a sinusoidal input with a frequency of 3.5 Hz (22 rad/s) and a magnitude of 0.03 m in this research. The tubular LBPMM was designed to be able to generate the force up to 29.6 N with a $\pm$6-A phase current [17]. Since the NdFeB magnet in the LBPMM would lose magnetization around 150°C, control performance is compromised with the maximum current swing that yields temperature rise. As a result, controllers are designed to have the current limit of around ± 4 A. The piezoelectric accelerometers (Piezotronics model 336B18) with the frequency range of 0.5 to 3000 Hz (3 to 20000 rad/s) used in our quarter-car test bed also limit the performance. Particularly, this implies that our active-suspension system is not able to attenuate the disturbance with a frequency component lower than 0.5 Hz.

The fact that this novel class of tubular LBPMM is used for active-suspension control as a force-generating component and three distinct control methodologies are developed, successfully implemented, and experimentally verified on a quarter-car model developed in our lab is the key contribution of this research and distinguishes this paper from others. Especially, an asymmetric fuzzy controller was implemented to compensate for the DC offset in sensor data. As for the control strategies, a modified lead-lag control was developed as a representative classical controller. Then an LQ servo controller was developed

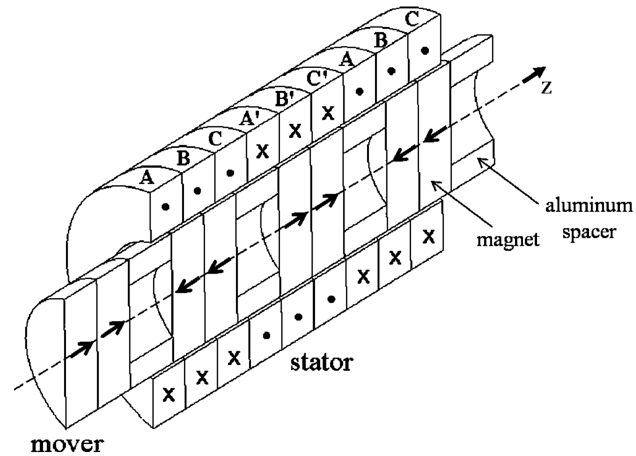

Fig. 1. Schematic of the tubular LBPMM. The direction of the generated force on the mover is in the negative z-direction in this particular current distribution.

to represent modern state-space-based control techniques. Lastly, fuzzy control was selected because of its flexibility with design parameter. The information such as the magnitude of the errors and the generated force gathered in the development of the previous two controllers facilitated the determination of its design parameters.

This paper is organized as follows. In Section II-A, working principles of the tubular LBPMM are summarized. Section II-B presents the modeling of the quarter-car test bed. In Section III-A, implementation of a modified lead-lag controller and its disturbance attenuation are presented. Section III-B describes the design and performance of an LQ servo controller and the state estimation by a Kalman filter. Section III-C presents a fuzzy controller with asymmetric membership functions and its performance. Section IV compares and analyzes the control performances of the three control strategies in detail. The conclusions follow in Section V.

II. Test Bed for Active Suspension Control

A. *Tubular Linear Brushless Permanent-Magnet Motor*

Fig. 1 shows a conceptual configuration of the tubular LBPMM. The mover of the LBPMM consists of a series of cylindrical permanent magnets. The magnets are fixed in a brass tube and connected with each other in an NS–NS—SN–SN fashion with spacers between the magnet pairs. The stator consists of 9 coils (3 per each phase). The three-phase coils are represented by A, B, and C in balanced three-phase operation. The magnets are aligned with the arrow pointing to the N pole. The pitch of these magnets is kept the same as that of the coils.

By the Lorentz force equation, the generated force is the vector cross product of the current density $\boldsymbol{J}$ in the coils and the magnetic flux density $\boldsymbol{B}$ generated by the magnets, $\boldsymbol{F} = \boldsymbol{J} \times \boldsymbol{B}$ [17]. The inverse Blondel-Park transformation in the LBPMM that governs the relationship between the three-phase currents and the desired force is defined as follows [17]:

$$\begin{bmatrix} i_a(t) \\ i_b(t) \\ i_c(t) \end{bmatrix} = C \begin{bmatrix} 2 & 0 \\ 1 & \sqrt{3} \\ -1 & \sqrt{3} \end{bmatrix} \begin{bmatrix} \cos\gamma_1 z_o \\ \sin\gamma_1 z_0 \end{bmatrix} f_{zd}(t) \qquad (1)$$

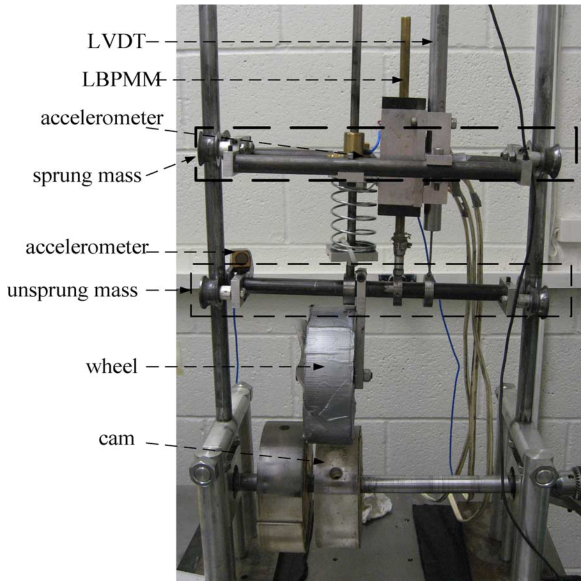

Fig. 2. Photograph of the quarter-car test bed with active suspension.

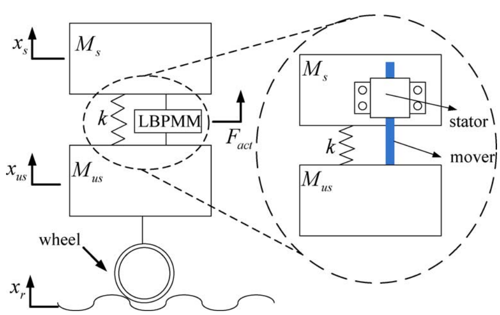

Fig. 3. Schematic diagram of the quarter-car test bed with active suspension.

TABLE I
PARAMETERS AND CORRESPONDING VALUES OF THE QUARTER-CAR

Parameters	Values
M_s	2.299 kg
M_{us}	2.278 kg
k	1521 N/m
c_w	50 N-s/m
k_w	156 N/m

where $i_a(t)$, $i_b(t)$, and $i_c(t)$ are the currents flowing in phases *A*, *B*, and *C*, respectively. f_{zd} is the desired force in the axial direction. $\gamma_1 = |2\pi/l|$, where l is the pitch of the motor (63.3 mm). z_0 is the relative displacement between the mover and the stator. In active suspension, it represents the distance between the sprung and unsprung masses. The inverse force constant C was determined as 0.1383 A/N by experiments [17].

B. Quarter-Car Test Bed

Fig. 2 shows a photograph of the quarter-car test bed. The sprung mass (M_s) is considered to be the body of a car, and the unsprung mass (M_{us}) represents the mass between its suspension and a wheel. As shown in Fig. 3, two masses are connected with a mechanical spring and the LBPMM. The stator of the LBPMM is fixed to the sprung mass and one end of the mover is fixed to the unsprung mass so that the LBPMM force can act on this quarter-car test bed. The rotating cam shown at the bottom of Fig. 2 simulates sinusoidal road disturbance at various frequencies.

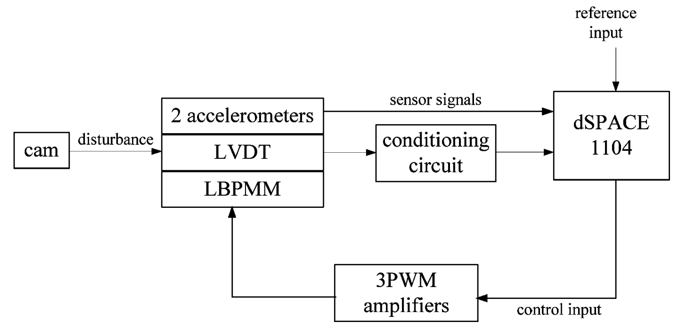

Fig. 4. Schematic diagram of the control architecture.

As in [16], the states of the quarter-car test bed are defined as $[\dot{x}_s(t) \quad \dot{x}_{us}(t) \quad x_s(t) - x_{us}(t) \quad x_{us}(t) - x_r(t)]^T$, and its dynamics is expressed as the following state-space matrix form:

$$\begin{bmatrix} \ddot{x}_s(t) \\ \ddot{x}_{us}(t) \\ \dot{x}_s(t) - \dot{x}_{us}(t) \\ \dot{x}_{us}(t) - \dot{x}_r(t) \end{bmatrix} = \begin{bmatrix} 0 & 0 & \frac{-k}{M_s} & 0 \\ 0 & \frac{-c_w}{M_{us}} & \frac{k}{M_{us}} & \frac{-k_w}{M_{us}} \\ 1 & -1 & 0 & 0 \\ 0 & 1 & 0 & 0 \end{bmatrix} \cdot \begin{bmatrix} \dot{x}_s(t) \\ \dot{x}_{us}(t) \\ x_s(t) - x_{us}(t) \\ x_{us}(t) - x_r(t) \end{bmatrix} + \begin{bmatrix} \frac{1}{M_s} \\ \frac{-1}{M_{us}} \\ 0 \\ 0 \end{bmatrix} F_{act}(t) + \begin{bmatrix} 0 \\ 0 \\ 0 \\ -1 \end{bmatrix} \dot{x}_r(t) \quad (2)$$

where $\dot{x}_s(t)$ and $\dot{x}_{us}(t)$ are the velocities of the sprung and unsprung masses, respectively, $x_r(t)$ is the sinusoidal disturbance generated by the rotating cam, and $F_{act}(t)$ is the force generated by the LBPMM. Additionally, the wheel is modeled by the spring constant k_w and the viscous damping coefficient c_w. The parameter values are given in Table I. The tire is assumed to be made of natural isoprene which has modulus of elasticity of 0.01 GPa.

Fig. 4 shows a schematic diagram of the control architecture. Analog-to-digital (A/D) channels on the dSPACE 1104 control board receive the sensor signals from the accelerometers and the LVDT. Controllers are implemented on this board and use the sensor signals for active suspension control. Since the A/D channels of the dSPACE 1104 board have an input voltage swing of ±10 V and the output swing of the LVDT is [0 V, 5 V], a conditioning circuit is used to shift the output range of the LVDT to match the input range of the A/D channels. Three PWM amplifiers are used to power the three-phase coils.

Since the disturbance is generated by the rotation of the cam with a fixed shape at a fixed speed, the magnitude of the disturbance could not be changed in this test bed. If a large disturbance should be generated by some reason, the LBPMM or the LVDT would not exceed the allowable operating range as long as the spring remains in its elastic region because the sprung mass and the unsprung mass are connected with each other through a mechanical spring.

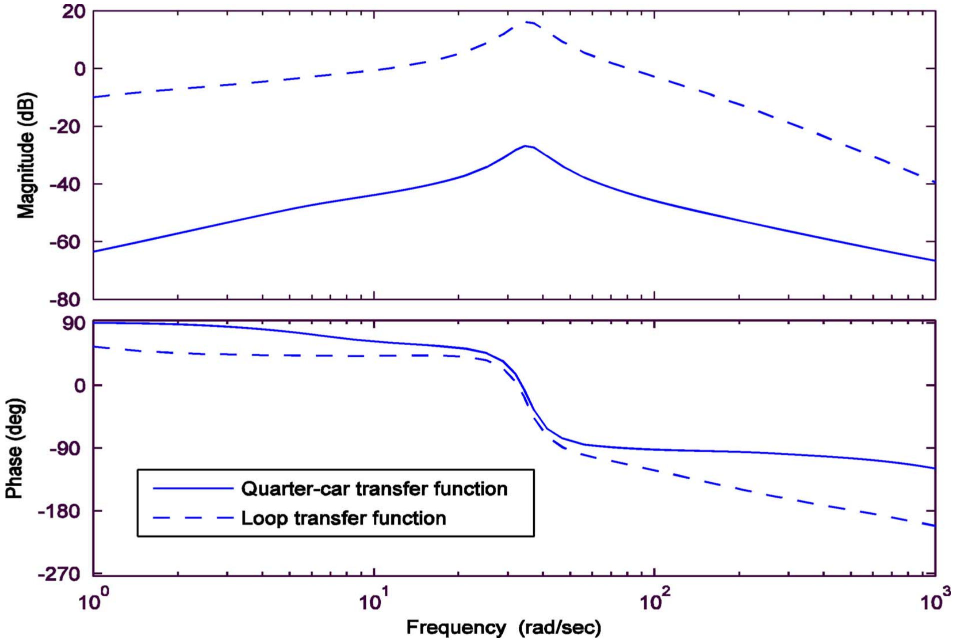

Fig. 5. Open-loop and loop-transfer-function frequency responses of the quarter-car dynamics (3) and the modified lead-lag controller (4). Gain and phase margins are 28.2 dB and 66.4°, respectively.

III. Control Strategies and Experimental Results

In this Section, three classes of controllers are designed and implemented in the quarter-car test bed and their experimental results are presented.

A. Modified Lead-Lag Control

The output of this modified lead-lag controller is a force and controls the velocity of the sprung mass rather than its position. Since the state-space-based control sets the velocity of the sprung mass as a reference input for the convenience of controller design [16], the same reference input is used in all control methodologies for fair comparison of their performances. From (2) and Table I, the transfer function from $F_{act}(t)$ to $\dot{x}_s(t)$ is determined as

$$G(s) = \frac{0.435s^3 + 9.547s^2 + 29.79s + 5.831 \times 10^{-14}}{s^4 + 21.95s^3 + 1398s^2 + 1.452 \times 10^4 s + 4.531 \times 10^4}. \tag{3}$$

The control objectives are as follows. First, a high loop gain is desirable around the operating frequency at 22 rad/s for good disturbance attenuation and command following. However, this high gain would yield large current flow in the LBPMM, which would raise its temperature and demagnetize the magnets. Therefore, the gain was limited by examining the simulation result of the maximum current flow (± 4 A) in the LBPMM. Finally, the loop gain of the controller at around the operating frequency was determined as 56 dB.

Second, the control bandwidth was set to be [10 rad/s, 80 rad/s]. Since the open-loop frequency response of this quarter car has low gains in the low and high frequency ranges and a high gain in the middle frequency range with two cross-over frequencies, the bandwidth could be adjusted by changing either the lower cross-over frequency or the higher cross-over frequency. In this paper, a lag compensator $((0.2252s + 1.15)/(s + 1.005))$ was applied in the low-frequency range to achieve this goal.

Third, since the gain should be low in the high frequency range to attenuate noise, another lag compensator $((0.04681s + 100.5)/(s + 100.54))$ was applied. Finally, to obtain sufficient gain and phase margins, a lead compensator $((1.949s + 100)/(s + 100.02))$ was introduced between the two lag controllers.

The lower-frequency lag controller yields a lower loop gain. The lead controller around the operating frequency broadens the bandwidth. Therefore, each lead or lag controller should be fine-tuned by examining the overall loop transfer function. To decide the exact corner frequencies in each of the lead or lag controllers, the Matlab SISO tool was used. The modified lead-lag controller with one lead and two lag controllers was finalized in the s domain as

$$C(s) = 12\frac{(s + 2147)(s + 51.31)(s + 5.107)}{(s + 100.54)(s + 100.02)(s + 1.005)}. \tag{4}$$

Fig. 5 shows the frequency responses of the open-loop transfer function and the loop transfer function. As seen in Fig. 5, the loop-transfer-function gain is much higher than that of the open-loop transfer function around the operating frequency (22 rad/s). The bandwidth is acceptable since it is close to the frequency range of [10 rad/s, 80 rad/s].

When the quarter-car test bed is under closed-loop control, the LBPMM generates the force to attenuate road disturbance, which results in the current flow in each coil set as shown in Fig. 6. Since the disturbance from the road is sinusoidal with a specified frequency, the current flow in the LBPMM would generate the force at the same frequency. However, each phase current exhibits some high-frequency distortions as shown in Fig. 6 due to unmodeled nonlinear dynamics in the system.

The simulation and experimental results of disturbance rejection are presented in Fig. 7. Due to the model uncertainties in

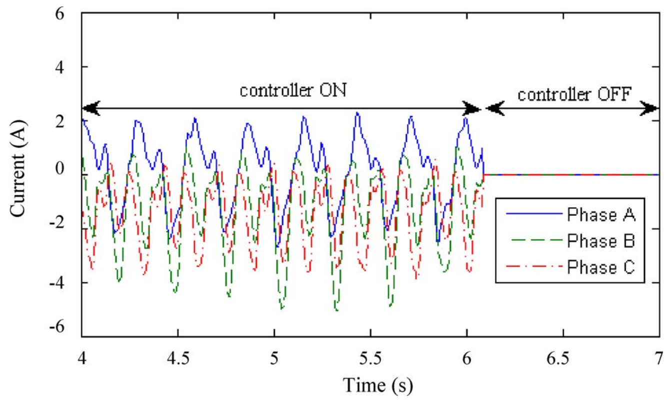

Fig. 6. Current flow of the modified lead-lag control in experiment for the 3.5 Hz (22 rad/s) disturbance. The LBPMM's phase currents are zero when the controller is turned off.

the quarter-car test bed, there is discrepancy between these two results. When the controller is turned off, the road disturbance affects directly to the quarter car, which results in high-velocity oscillation of the sprung mass. When the controller is turned on, the road disturbance is attenuated.

Fig. 8 shows the acceleration of the sprung mass in simulation and experiment. In this figure, the magnitude of the sprung-mass acceleration is much smaller when the controller is turned on than off. This implies that the road disturbance affects the rider less in terms of the acceleration as well.

B. Linear-Quadratic Servo Control

LQ servo control is developed by introducing the command input and the output disturbance. From (2), a state-space representation of a quarter-car model can be expressed as follows:

$$\begin{aligned} \dot{\boldsymbol{x}}_{\boldsymbol{p}}(t) &= A_p \boldsymbol{x}_{\boldsymbol{p}}(t) + B_P u(t) \\ y_p(t) &= C_p \boldsymbol{x}_{\boldsymbol{p}}(t) \end{aligned} \tag{5}$$

where

$$\boldsymbol{x}_{\boldsymbol{p}}(t) = [\dot{x}_s(t) \quad \dot{x}_{us}(t) \quad x_s(t) - x_{us}(t) \quad x_{us}(t) - x_r(t)]^T,$$

$$A_p = \begin{bmatrix} 0 & 0 & -k/M_s & 0 \\ 0 & -c_w/M_{us} & k/M_{us} & -k_w/M_{us} \\ 1 & -1 & 0 & 0 \\ 0 & 1 & 0 & 0 \end{bmatrix}$$

$$B_p = \begin{bmatrix} 1/M_s \\ -1/M_{us} \\ 0 \\ 0 \end{bmatrix} \qquad C_p = \begin{bmatrix} 1 \\ 0 \\ 0 \\ 0 \end{bmatrix}^T$$

as in (2). Thus, $y_p(t) = \dot{x}_s(t)$ and $\boldsymbol{x}_{\boldsymbol{p}}(t)$ is partitioned as follows:

$$\begin{aligned} \boldsymbol{x}_{\boldsymbol{p}}(t) &= \left[y_p(t) \,|\, \boldsymbol{x}_{\boldsymbol{R}}^T(t) \right]^T \\ &= [\dot{x}_s(t) \,|\, \dot{x}_{us}(t) \quad x_s(t) - x_{us}(t) \quad x_{us}(t) - x_r(t)]^T. \end{aligned} \tag{6}$$

The vertical line indicates that $y_p(t) = \dot{x}_s(t)$. The last state is the relative displacement between the sprung mass and the unsprung mass. It can be easily measured by the LVDT.

As shown in Fig. 9, the control gain matrices G_y and G_r are applied to $y_p(s)$ and $\boldsymbol{x}_{\boldsymbol{R}}(s)$, respectively. To eliminate a non-zero steady-state error for the step command input or the output disturbance, this LQ servo controller is implemented with an integrator. In this application, the LQ servo model is determined by considering the frequency responses of the loop transfer functions as given in Fig. 10.

Fig. 10 shows the loop transfer functions of a standard LQ servo model (*i.e.,* model *a*) and an LQ servo model with an integrator (*i.e.,* model *b*). The most significant difference between these two models is the low frequency response. Model *b* has the magnitude slope of 20 dB/decade around the lower cross-over frequency. Model *a* has larger slope than 20 dB/decade around the lower cross-over frequency. Therefore, the magnitude of the sensitivity function of model *a* is smaller than model *b*. Model *a* is desirable in terms of disturbance rejection and command following. However, improvement of the sensitivity in a frequency range deteriorates the sensitivity in another frequency range. The system could also become unstable due to this deterioration [23]. Since the operating frequency of the quarter car is around 22 rad/s, improvement of the sensitivity in the frequency range less than 22 rad/s is not as significant a factor as the stability of the system. Therefore, model *b* is more suitable for the quarter car than model *a*.

Its control objectives are similar to those of the modified lead-lag control. First, loop gains should be high around the operating frequency. Second, the control bandwidth should be located in [10 rad/s, 80 rad/s]. The control objectives are more conveniently achievable with model *b* than model *a* because it has an additional design parameter (G_i). This also gives the relevance to the usage of the integrator.

As shown in Fig. 9, the control gains for the integrator, output state, and rest states are G_i, G_y, and G_r, respectively [24]. This LQ servo system consisted of the standard LQ servo dynamics (5) and the integrator dynamics. With $r(s) = 0$ in a regulation problem

$$z_p(s) = -\frac{1}{s} y_p(s) = -\frac{1}{s} \dot{x}_s(s). \tag{7}$$

The augmented system is defined as follows:

$$\dot{\boldsymbol{x}}(t) = A\boldsymbol{x}(t) + Bu(t) \tag{8}$$

where $\boldsymbol{x}(t) = \left[z_p(t) \;\; y_p(t) \;\; \boldsymbol{x}_{\boldsymbol{R}}^T(t) \right]^T$, $A = \begin{bmatrix} 0 & -C_P \\ 0 & A_P \end{bmatrix}$, and $B = [0 \quad B_p{}^T]^T$. The control law is defined as

$$u(t) = -G\boldsymbol{x}(t) \tag{9}$$

where $G = [G_i \quad G_y \quad G_r]$.

To obtain G, a control algebric Riccati equation (CARE) should be solved. To construct this CARE, a symmetric positive definite matrix R and a symmetric positive semi-definite matrix Q should be determined. The R matrix affects the loop gain that determines the system bandwidth. The maximum current flow is constrained as ± 4 A, the same as the case of the modified lead-lag controller. After several design iterations, R was set to be 0.005. The diagonal elements of the Q matrix are the weights of each state, and they determine the shape of the loop transfer

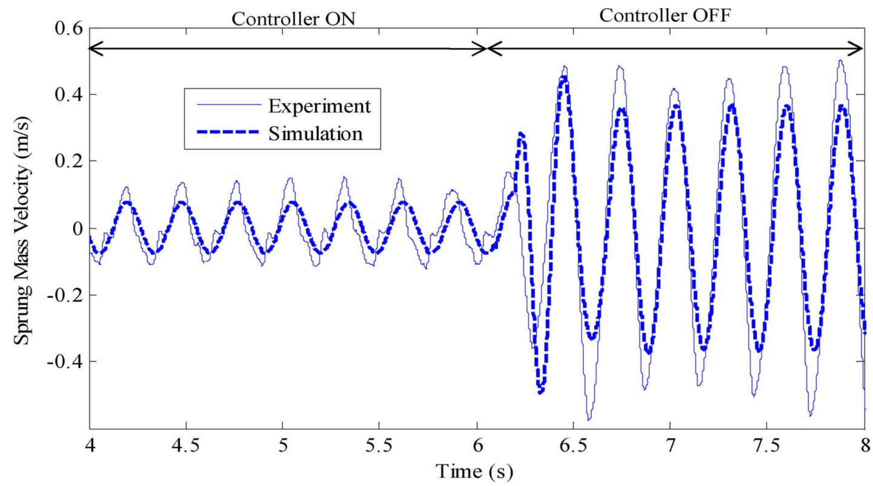

Fig. 7. Experiment and simulation results of the modified lead-lag control (4) for the 3.5 Hz disturbance.

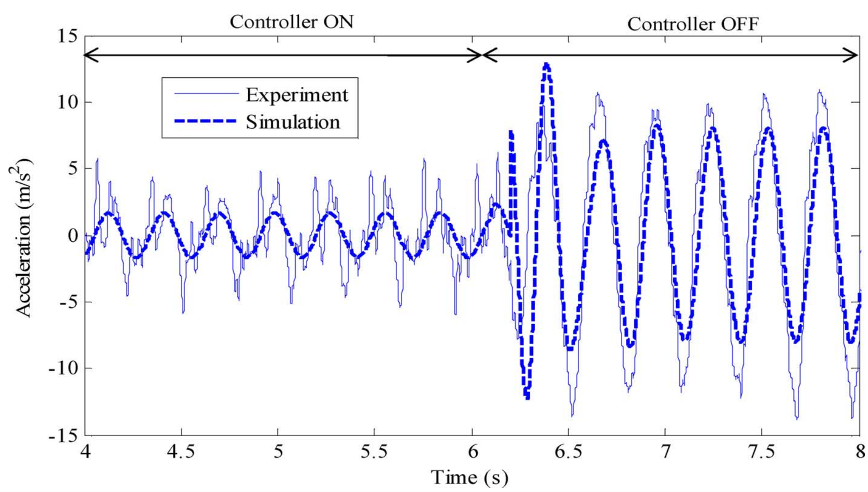

Fig. 8. Sprung mass accelerations with the modified lead-lag control.

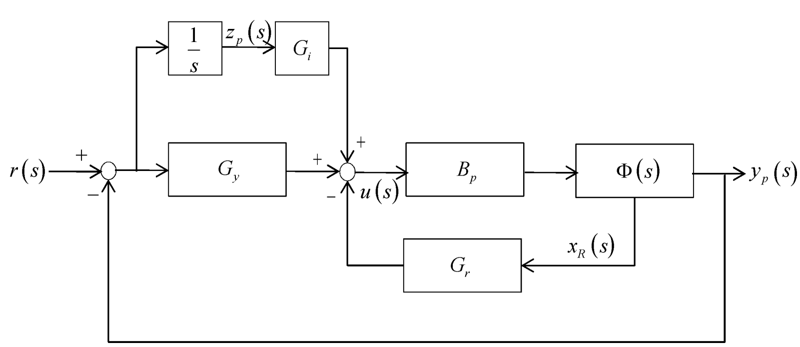

Fig. 9. Block diagram of the LQ servo control.

function. Since the second state $(\dot{x}_s(t))$ should be regulated, the Q matrix is desirable to have a larger element $Q(2,2)$ than other elements in the Q matrix. After several design iterations, the Q matrix was determined as follows:

$$\begin{aligned} diag\,(Q) &= [0.01 \quad 170 \quad 0.01 \quad 0.01 \quad 0.01] \\ Q_{ij} &= 0 \ (i \neq j). \end{aligned} \tag{10}$$

A unique positive semi-definite symmetric matrix K is determined by solving the following CARE:

$$-KA - A^TK - Q + KBR^{-1}B^TK = 0. \tag{11}$$

K is found with Matlab as follows:

$$K = \begin{bmatrix} 1.1078 & 0 & 0 & -1.1078 & -1.1078 \\ 0 & 0 & 0 & -0.0003 & 0 \\ 0 & 0 & 0 & -0.0003 & 0 \\ -1.1078 & -0.0003 & -0.0003 & 1.1190 & 1.1104 \\ -1.1078 & 0 & 0 & 1.1104 & 1.1102 \end{bmatrix}. \tag{12}$$

The feedback gain G is determined as follows:

$$G = R^{-1}BK = [0.0013 \;\; 147.58 \;\; -25.7212 \;\; 0 \;\; 272.5471]. \tag{13}$$

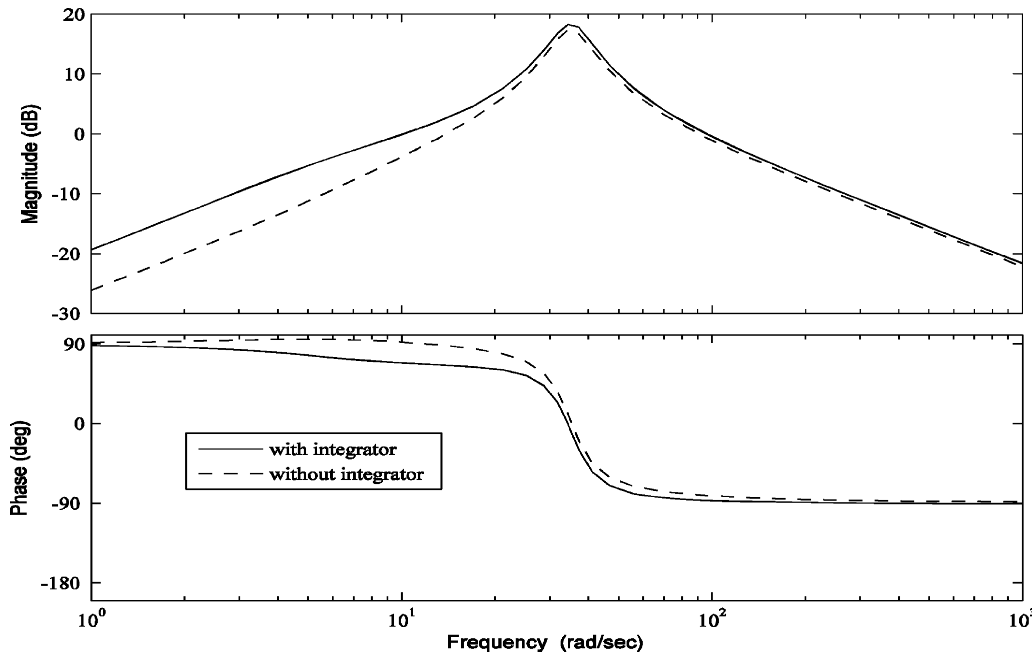

Fig. 10. Frequency responses of the loop transfer functions in the LQ servo control.

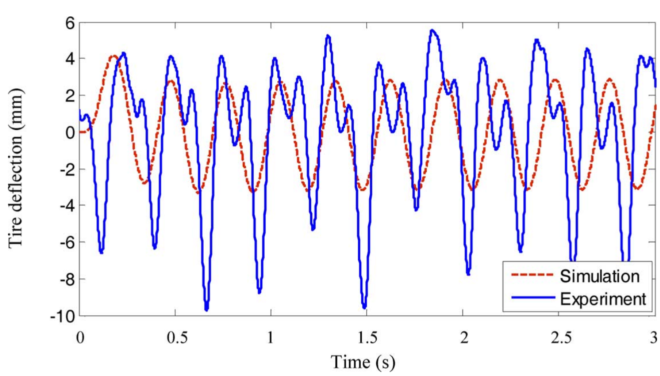

Fig. 11. Estimated state comparison between simulation and experiment results.

Fig. 10 (solid line) is the frequency response of the loop transfer function with the feedback gains from (13).

1) Kalman Filter Design: An LQ servo requires full state feedback. The last state is defined as the tire deflection $(x_{us}(t)-x_r(t))$, which is difficult to measure and estimate with a Kalman filter. This estimator requires the measured output $(\dot{x}_s(t))$ and the system control input $F_{act}(t)$ as an estimator input. To solve the filter algebric Riccati equation (FARE) and obtain the Kalman-filter gain, a positive value Θ and a non-negative value Ξ should be determined as

$$AP + PA^T + L\Xi L^T - PC^T\Theta^{-1}CP = 0. \tag{14}$$

As expressed in (2), the output disturbance affects the last state of the quarter-car model. Therefore, the matrix L is defined as follows:

$$L = [0 \quad 0 \quad 0 \quad -1]^T. \tag{15}$$

With initial values of $\Theta = 1$ and $\Xi = L^T L$, they were adjusted and determined as $\Theta = 0.00001$ and $\Xi = 0.01$ after several design iterations. Then the unique positive semi-definite symmetric matrix P is obtained as follows with the Matlab CARE function:

$$P = \begin{bmatrix} 0.0005 & 0.0004 & 0 & -0.0003 \\ 0.0004 & 0.0012 & 0 & -0.0008 \\ 0 & 0 & 0 & 0 \\ -0.0003 & -0.0008 & 0 & 0.0007 \end{bmatrix}. \tag{16}$$

The Kalman-filter gain H is determined as follows:

$$H = PC^T\Theta^{-1} = [46.9286 \quad 41.9643 \quad -1.6644 \quad -28.9742]. \tag{17}$$

Fig. 11 shows the estimated tire deflection $(x_{us}(t) - x_r(t))$ by the Kalman filter algorithm in closed-loop control. There is some discrepancy between the simulation and experimental results of state estimation. In the Kalman filter algorithm, the measured output and the disturbance are assumed as zero-mean white Gaussian noises. In the quarter-car model, there is some discrepancy between the measured output $(\dot{x}_s(t))$ and the zero-mean white Gaussian noise (Figs. 7 and 12(a)), which limits the performance of the state estimator. The performance of the disturbance attenuation in velocity is presented in Fig. 12(a).

Two accelerometers and one LVDT are used as sensors in LQ servo controller. Due to the noises generated by the sensors and the error from the state estimator, disturbance attenuation contains some discrepancy between the experiment and simulation results. Fig. 12(b) shows the acceleration of the sprung mass.

C. Fuzzy Control

A Mamdani-type fuzzy controller is implemented in this section [25]. The input to this fuzzy controller is the system error $(e(t))$ and the output is the control input $(F_{act}(t))$. To determine $F_{act}(t)$, $e(t)$ is fuzzified by the membership functions as shown in Fig. 13(a) and defuzzified by the membership functions as shown in Fig. 13(b). The membership functions

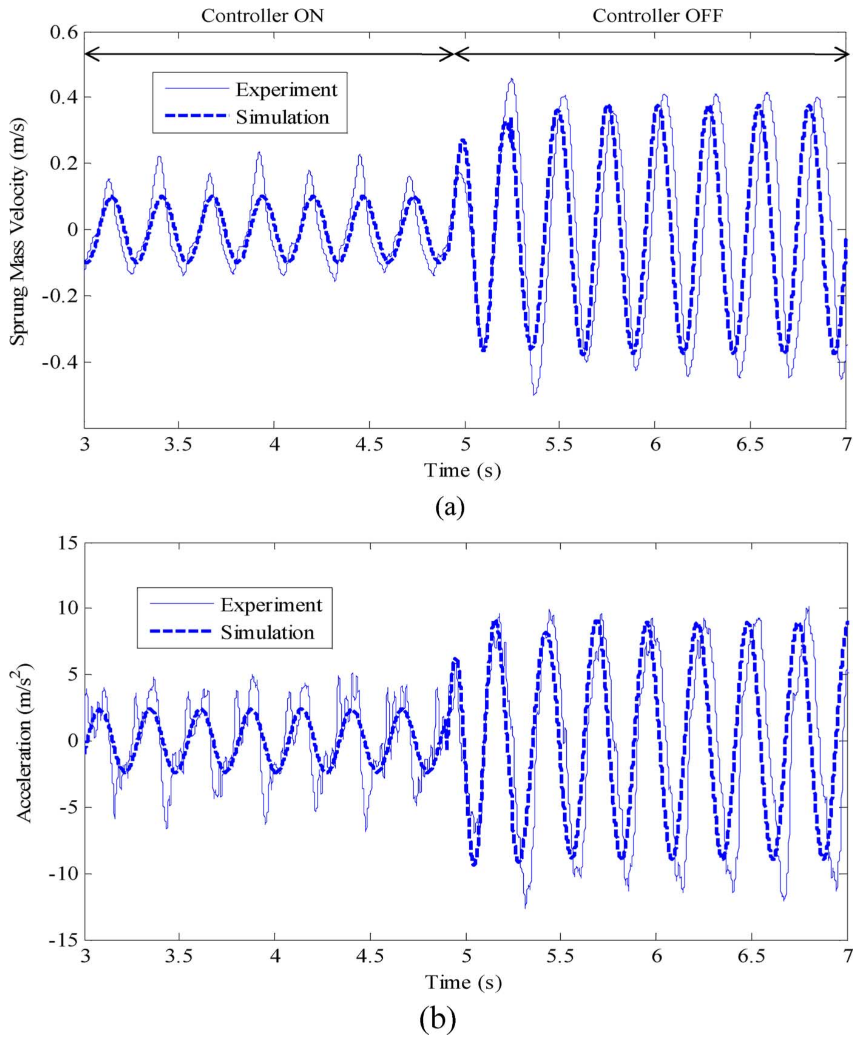

Fig. 12. (a) Experiment and simulation results of the LQ servo control when the controller is turned on. (b) Sprung mass accelerations with the LQ servo control.

for the fuzzification are denoted according to the amount of the error: NLE (Negative Large Error), NME (Negative Medium Error), NSE (Negative Small Error), ESE (Evenly Small Error), PSE (Positive Small Error), PME (Positive Medium Error), and PLE (Positive Large Error). For defuzzification, membership functions are denoted according to the force generated by each membership function: NLF (Negative Large Force), NMF (Negative Medium Force), NSF (Negative Small Force), ESF (Evenly Small Force), PSF (Positive Small Force), PMF (Positive Medium Force), and PLF (Positive Large Force). The area under the membership functions (NLF, NMF, NSF, ESF, PSF, PMF, PLF) are defined by μ_i $(i = 1,\ 2,\ \ldots, 7)$.

The range of error in Fig. 13(a) was set as $[-0.8, 0.8]$ because the magnitude of the largest measured error ($|\dot{x}_s(t)|$) was 0.8 m/s. The range of outputs in Fig. 13(b) was set as $[-30, 30]$ because the LBPMM could generate force up to near ± 30 N.

As presented in Fig. 13, seven membership functions were implemented for the fuzzification and defizzification. Several controllers with the different number of membership functions were tested, and the one with seven membership functions was selected since it exhibited the best result without requiring complexity.

Table II shows the rules of this fuzzy controller. Since this active-suspension test bed is a single-input, single-output system, the input and the output forms single-dimension arrays. Each fuzzified value is one-to-one matched for the defuzzification. For example, if the error is NLE, the output is NLF. Each rule has the same weight.

The control input as the result of this fuzzy controller is determined by the center of gravity (COG) method. The COG method computes F_{act} as follows [22]:

$$F_{act} = \frac{\sum_{i=1}^{7} g_i \int \mu_i}{\sum_{i=1}^{7} \int \mu_i} \tag{18}$$

where g_i is defined as the COG of the each membership function.

Fig. 14 shows the relation between the error (input) and the generated control force (output). This input-output curve was designed not to be symmetric with respect to the origin. The characteristics of error due to non-idealities of the test bed is presented as follows:

$$\max\{|\dot{x}_s(t)|| \dot{x}_s(t) > 0\} > \max\{|\dot{x}_s(t)|| \dot{x}_s(t) < 0\}. \tag{19}$$

When the active-suspension system is under closed-loop control, the maximum absolute velocity of the sprung mass is larger

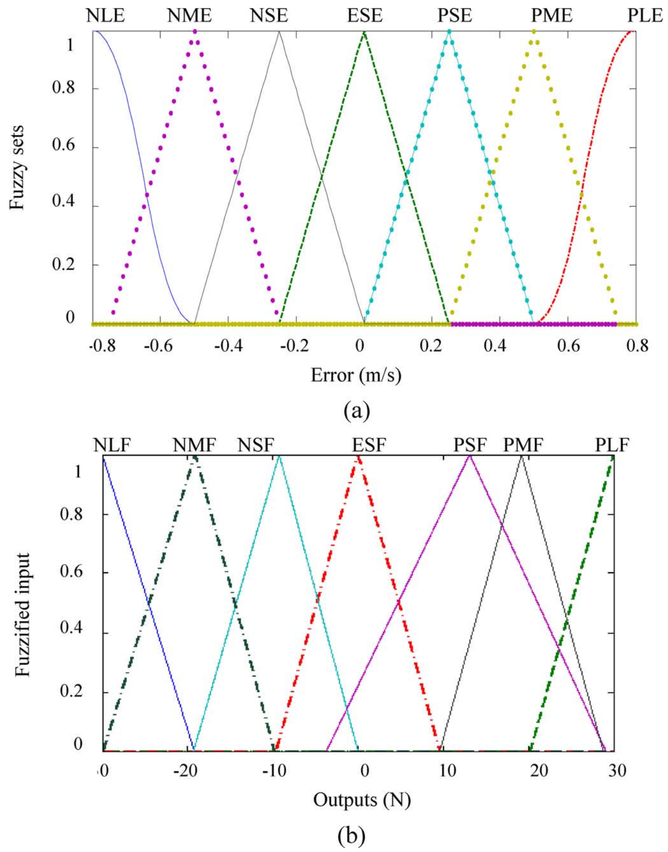

Fig. 13. (a) Membership functions for fuzzification. (b) Membership functions for defuzzification.

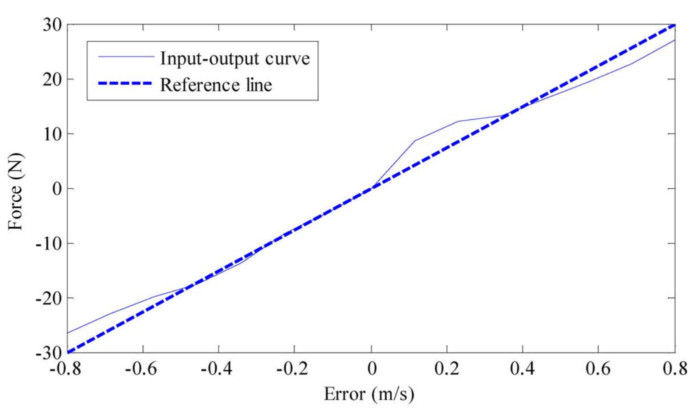

Fig. 14. Input-output relation of the asymmetric fuzzy controller.

when it is positive than negative (i.e., peak toward positive is larger than peak toward negative). The phenomenon of (19) was examined through the modified lead-lag control and the LQ servo control (Figs. 7 and 12(a)). This indicates that the position of the sprung mass is higher than the desired position. It also means an insufficient control input to attenuate disturbance when the sprung mass moves upward. Therefore, additional control input should be generated to reduce the error when $\dot{x}_s(t) > 0$. The mechanical spring between the spung mass and the unsprung mass might cause this phenomenon. Since this mechanical spring has initial tension when it is extended but does not have it when compressed, required force to regulate the spring motion may be different depending on compression or extension.

TABLE II
RULES OF THE FUZZY CONTROLLER

Force \ Error	NLE	NME	NSE	ESE	PSE	PME	PLE
NLF	1	0	0	0	0	0	0
NMF	0	1	0	0	0	0	0
NSF	0	0	1	0	0	0	0
ESF	0	0	0	1	0	0	0
PSF	0	0	0	0	1	0	0
PMF	0	0	0	0	0	1	0
PLF	0	0	0	0	0	0	1

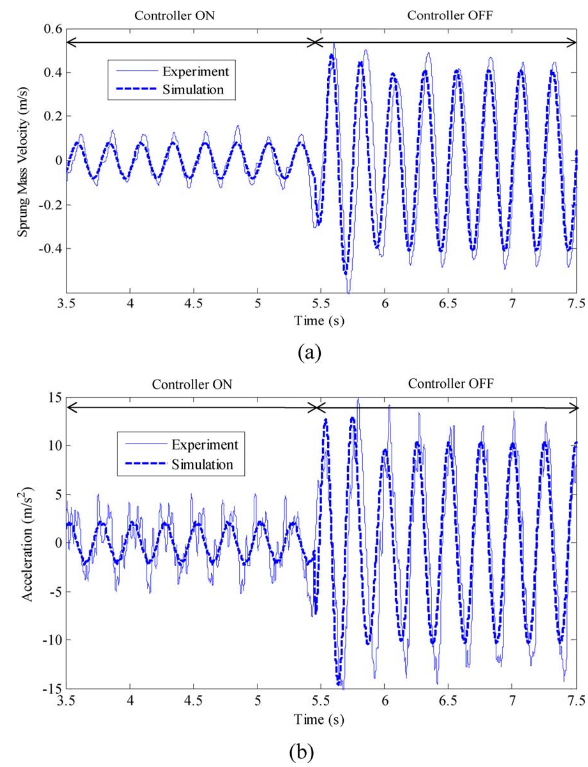

Fig. 15. (a) Fuzzy control result of experiment and simulation when controller is turned on. (b) Sprung mass accelerations with the fuzzy control.

To solve the problem presented as (19), a membership function PSF in Fig. 13(b) is widened. The PSF is the most significant membership function when the system is under closed-loop control because the domain of the PSE covers a small negative error and the PSF is determined by the PSE. The widened PSF induces the increased area of the PSF(μ_3). Consequently, the absolute value of the COG of the PSF increased. Finally, F_{act} also increased by (18) when $0.1 < \mathrm{Error}\ (\mathrm{m/s}) < 0.4$.

In Fig. 15(a), the effect of (19) is reduced in comparison with Figs. 7 and 12(a) due to the additional control input generated in the hump where $0.1 < \mathrm{Error}\ (\mathrm{m/s}) < 0.4$ in Fig. 14. Fig. 15(b) shows the acceleration of the sprung mass.

IV. Performance Comparisons

We presented three control strategies of active-suspension control in this paper. The modified lead-lag controller is a kind of classical controller and the LQ servo controller is a state-

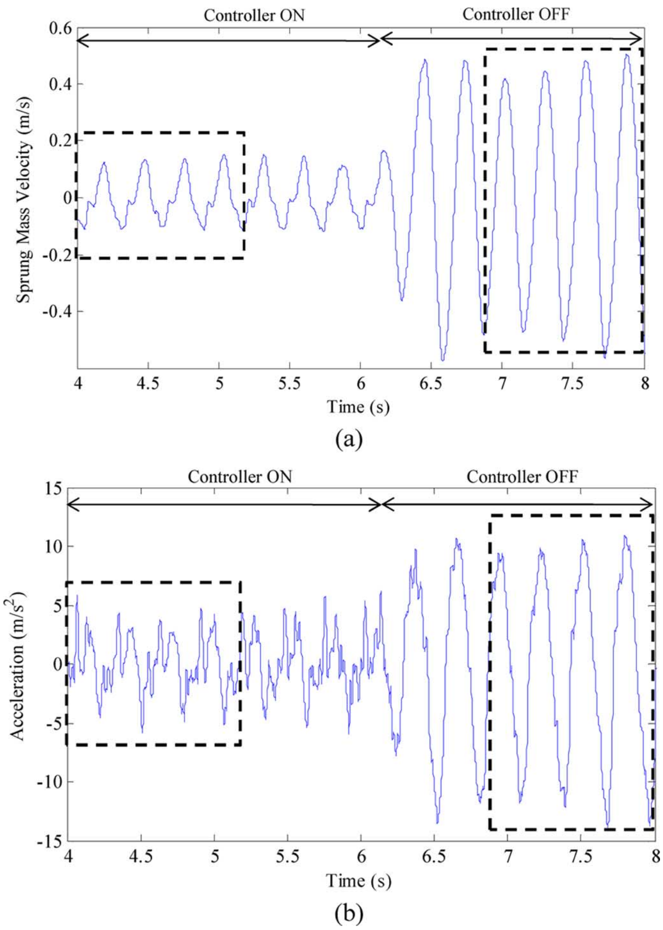

Fig. 16. Data samples used for performance evaluation of the sprung mass. (a) Velocity and (b) acceleration in the modified lead-lag control.

space based modern controller. The development of the fuzzy controller was based on the membership functions. However, these controllers have the same objective to attenuate the road disturbance. Therefore, one aspect that can be compared among these controllers is the disturbance-attenuation performance. In this section their disturbance-attenuation performance is compared in terms of the sprung mass velocity and acceleration.

Fig. 16 shows the data samples collected for performance evaluation in the modified lead-lag control. Samples are gathered in the steady-state regions only. Dashed boxes on the left and right sides are the samples when the controller is on and off, respectively. Three-thousand discrete data points were collected in each case.

Once the samples are obtained, the root-mean-square (RMS) values are calculated in velocity when the controller is on and off. The RMS values are calculated also in acceleration when the controller is on and off as follows:

$$\text{Lead-lag}_{\text{vel.RMS}} = \sqrt{\frac{1}{n}\sum_{i=1}^{n}\dot{x}_s(t)^2}$$
$$\text{Lead-lag}_{\text{acc.RMS}} = \sqrt{\frac{1}{n}\sum_{i=1}^{n}\ddot{x}_s(t)^2} \quad (20)$$

TABLE III
PERFORMANCE COMPARISON

Controllers	Values	Acceleration	Velocity
Modified lead-lag	RMS on	2.323 m/s^2	0.075 m/s
	RMS off	7.482 m/s^2	0.283 m/s
	Performance Index	67 %	73 %
LQ servo	RMS on	2.855 m/s^2	0.099 m/s
	RMS off	6.854 m/s^2	0.276 m/s
	Performance Index	58 %	64 %
Fuzzy	RMS on	2.576 m/s^2	0.071 m/s
	RMS off	8.413 m/s^2	0.310 m/s
	Performance Index	69 %	77 %

where $\dot{x}(t)$ and $\ddot{x}(t)$ are the sprung-mass velocity and acceleration, respectively and n is the number of the sample data ($n = 3000$). Then the performance indicies are calculated from the RMS values as follows:

$$\text{Perf.Ind.}_{\text{vel\_lead-lag}} = \left(1 - \frac{\text{Lead-lag}_{\text{vel.RMS\_ON}}}{\text{Lead-lag}_{\text{vel.RMS\_OFF}}}\right) \times 100. \quad (21)$$

The performance indicies show how much the controller was able to attenuate the road disturbance in sprung mass velocity and acceleration. In the same way, performance indicies are calculated in the case of LQ servo and fuzzy control. Table III shows the comparison.

In case of the modified lead-lag control, the RMS values of the sprung mass acceleration were 2.323 and 7.482 m/s^2 when the controller is on and off, respectively. The corresponding performance index was 67%, which means that 67% of the disturbance from the road is attenuated in the sprung mass acceleration. Similarly, the RMS values of the sprung mass velocity were 0.075 and 0.238 m/s when the controller is on and off, respectively and corresponding performance index was 73%. When the controllers were on, the RMS values for the modified lead-lag, LQ servo, and fuzzy controllers were 0.075, 0.099, and 0.071 m/s. The smallest RMS value from the fuzzy controller implies that the DC offset was reduced due to the asymmetric membership function.

The current flow pattern in the tubular LBPMM with the modified lead-lag controller is shown in Fig. 17. Since each phase has 60° differences, the phase A current has the same magnitude but opposite direction to the phase B and C currents.

Considering this symmetry, how much control input was required in this controller was calculated by taking the RMS value of the phase A current as follows:

$$\text{Current}_{A.\text{RMS}} = \sqrt{\frac{1}{n}\sum_{i=1}^{n} {I_A}^2(t)} \quad (22)$$

where $I_A(t)$ is the phase A current, n is the number of sampled data ($n = 3000$). Similarly, the RMS values of the phase A currents were obtained in case of the LQ servo and the fuzzy control. Table IV shows this result.

A small RMS value in Table IV means a small control input. The modified lead-lag and the fuzzy controllers required almost the same amount of the control input, which were 1.26 and 1.24

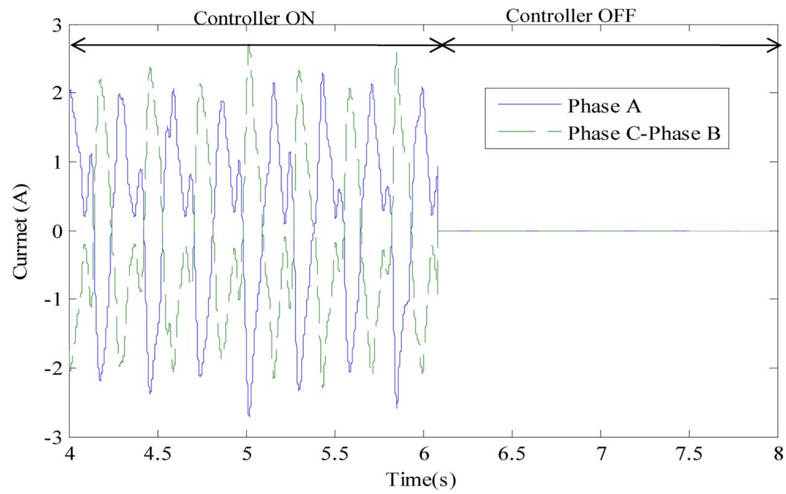

Fig. 17. Current flow pattern in each coil set with the modified Lead-lag control.

TABLE IV
RMS VALUES OF THE CURRENT FLOW IN PHASE A

Controllers	RMS values
Modified Lead-Lag	1.26 A
LQ servo	1.33 A
Fuzzy	1.24 A

A, respectively. However, the LQ servo required more control input then the other two controllers.

V. CONCLUSION

An active-suspension system with a quarter-car test bed was constructed with a tubular LBPMM in this research. Modified lead-lag, LQ servo, fuzzy controllers were designed and implemented to attenuate road disturbance. The modified lead-lag and LQ servo controllers showed 67% and 58% in the disturbance-attenuation performance, respectively in the sprung mass acceleration. The fuzzy controller was able to reject the disturbance by up to 69% in the sprung mass acceleration. In the sprung mass velocity, the modified lead-lag, LQ servo, and fuzzy controller attenuated the road disturbance by 73%, 64%, and 77%, respectively. Overall performance in the sprung mass velocity was superior to acceleration because these controllers were originally designed to attenuate the sprung mass velocity.

The LQ servo's performance in disturbance rejection was slightly inferior to the two other controllers. The reason is that the estimator could not perfectly generate the estimated state because the noise and the disturbance were not white Gaussian. Moreover, an additional sensor (the LVDT) was used in this control method. Therefore, both performance- and cost-effectiveness-wise, the LQ servo was not suitable for this application. The performance of the modified lead-lag control was fairly acceptable. It consisted of two lag controllers and one lead controller. Each lead and lag controller was designed to satisfy its own control objectives. Finally, these lead and lag controllers were fine-tuned to determine their exact corner frequencies. Selecting its design parameters did not require too many design iterations to satisfy the control objectives. In addition, this modified lead-lag control required no LVDT. The performance of the fuzzy controller was the best among the three controllers with 77% in the sprung mass velocity and 69% in acceleration. It is because this controller is developed so that it can compensate for the DC offset by introducing asymmetric membership functions. However, the development of this fuzzy controller requires the information such as the magnitude of the errors and the generated force gathered during the development of the two previous controllers. When it comes to the current flow, the modified lead-lag controller and the fuzzy controller required almost the same control input. However, the LQ servo controller required more control input although its performance was inferior to the other two controllers.

In summary, the tubular LBPMM, a unique tubular linear motor, was successfully employed as an actuator in active-suspension control. When it comes to the control performance, the fuzzy controller turned out to be the most suitable control methodology for this active-suspension application. It is because its asymmetric membership functions allowed the tubular LBPMM to generate the most suitable control force. Due to the asymmetric membership functions, the discrepancy between the ideal and practical test beds was reduced. However, a fuzzy controller is difficult to design since it has infinitely many design parameters such as selecting the domain for the fuzzification and defuzzyfication. In this research, these design parameters were finalized with the results from the modified lead-lag and LQ servo controllers.

REFERENCES

[1] J. Allen, "Design of active suspension control based upon use of tubular linear motor and quarter-car model," Master's thesis, Texas A&M Univ., College Station, TX, 2008.
[2] H. Peng, R. Stratharn, and A. Ulsoy, "A novel active suspension design technique–simulation and experimental results," in *Proc. 1997 Amer. Contr. Conf.*, Jun. 1997, pp. 709–713.
[3] C. Tang and T. Zhang, "The research on control algorithms of vehicle active suspension system," in *Proc. IEEE Int. Conf. Veh. Electron. Safety*, Oct. 2005, pp. 320–325.
[4] Y. M. Sam, M. R. H. A. Ghani, and N. Ahmad, "LQR controller for active car suspension," in *Proc. TENCON 2000*, Sep. 2000, pp. 441–444.
[5] C. Lauwerys, J. Swevers, and P. Sas, "Design and experimental validation of a linear robust controller for an active suspension of a quarter-car," in *Proc. 2004 Amer. Contr. Conf.*, Jul. 2004, pp. 1481–1486.

[6] J. Wang, A. C. Zolas, and D. A. Wilson, "Active suspension: A reduced-order H_∞ control design study," in *Proc. Mediterranean Conf. Contr. Automat.*, Jul. 2007, pp. 132–140.
[7] J. Concha and A. Cipriano, "A design method for stable fuzzy LQR controllers," in *Proc. 6th IEEE Int. Conf.*, Jul. 1997, vol. 1, pp. 271–276.
[8] M. Gobbi, F. Levi, and G. Mastinu, "Multi-objective stochastic optimization of the suspension system of road vehicles," *J. Sound Vibration*, vol. 298, no. 4, pp. 1055–1072, Dec. 2006.
[9] S. Savaresi, E. Silani, and S. Bittanti, "Acceleration-driven-damper (ADD): An optimal control algorithm for comfort-oriented semi-active suspensions," *J. Dynamic Syst., Measure. Contr.*, vol. 127, no. 2, pp. 218–229, Jul. 2005.
[10] S. Savaresi and C. Spelta, "Mixed sky-hook and ADD: Approaching the filtering limits of a semi-active suspension," *J. Dynamic Syst., Measure. Contr.*, vol. 129, no. 4, pp. 382–392, Jul. 2007.
[11] S. Savaresi and C. Spelta, "A single-Sensor control strategy for semi-active suspensions," *IEEE Trans. Contr. Syst. Technol.*, vol. 17, pp. 143–152, Jan. 2009.
[12] C. Abbas, T. Rahaijaona, and H. Noura, "Sliding mode control applied to active suspension using nonlinear full vehicle and actuator dynamics," in *Proc. 2006 IEEE Conf. Decision Contr.*, Dec. 2006, pp. 3597–3602.
[13] Y. Jin, D. Yu, and X. Song, "An integrated-error-based adaptive neuron control and its application to vehicle suspension systems," in *Proc. IEEE Int. Conf. Contr. Automat.*, May 2007, pp. 564–569.
[14] F. Kou and Z. Fang, "An experimental investigation into the design of vehicle fuzzy active suspension," in *Proc. IEEE Int. Conf. Automat. Logist.*, Aug. 2007, pp. 959–963.
[15] A. Alleyne and J. Hedrick, "Nonlinear adaptive control of active suspension," *IEEE Trans. Contr. Syst. Technol.*, vol. 3, pp. 91–101, Mar. 1995.
[16] R. Rajamani, "Adaptive observers for active automotive suspensions: Theory and experiment," *IEEE Trans. Contr. Syst. Technol.*, vol. 3, pp. 86–93, Mar. 1995.
[17] W.-J. Kim and B. Murphy, "Development of a novel direct-drive tubular linear brushless permanent-magnet motor," *Int. J. Contr., Automat., Syst.*, vol. 2, no. 3, pp. 279–288, Sep. 2004.
[18] R. Williams, "Control of a low frequency active suspension," in *Proc. Int. Conf. Contr.*, Mar. 1994, vol. 1, pp. 338–343.
[19] M. Hoque, M. Yakasaki, Y. Ishino, and T. Mizuno, "Design of a mode-based controller for 3-DOF vibration isolation system," in *Proc. IEEE Int. Conf. Robot., Automat. Mechatron.*, Dec. 2004, pp. 478–483.
[20] H. Gao, J. Lam, and C. Wang, "Multi-objective control of vehicle active suspension systems via load-dependent controllers," *J. Sound Vibration*, vol. 290, no. 7, pp. 654–675, Mar. 2006.
[21] N. Yagiz, I. Yuksek, and S. Sivrioglu, "Robust control of active suspensions for a full vehicle model using sliding mode control," *Int. J. Jpn. Soc. Mechan. Eng.*, vol. 43, no. 2, pp. 253–258, Jul. 2000.
[22] Y. Suda and T. Shiba, "A new hybrid suspension system with active control and energy regeneration," *Int. J. Veh. Mechan. Mobil.*, vol. 25, no. 1, pp. 641–654, Jan. 1996.
[23] G. Stein, "Respect the unstable," *IEEE Contr. Syst. Mag.*, vol. 23, no. 4, pp. 12–25, Aug. 2003.
[24] B. Anderson and J. Moore, *Optimal Control: Linear Quadratic Methods*. Englewood Cliffs, NJ: Prentice-Hall Int., 1989, p. 74.
[25] K. Passino and S. Yurkovich, *Fuzzy Control*. Boston, MA: Addison-Wesley, 1999, p. 42.

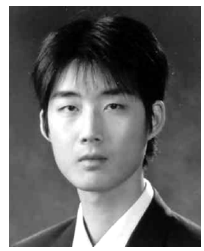

Seungho Lee (S'08) received the B.S. degree in computer science and mechanical engineering from Yonsei University, Seoul, Korea, in 2001 and 2005, respectively. In 2009, he received the M.S. degree in mechanical engineering from the Texas A&M University, College Station. Currently, he is pursuing the Ph.D. degree in mechanical engineering at the University of Illinois at Urbana-Champaign.

His research interests include analysis and design of control systems.

Won-jong Kim (S'89–M'97–SM'03) received the B.S. (*summa cum laude*) and M.S. degrees from Seoul National University, Seoul, Korea, in 1989 and 1991, respectively, and the Ph.D. degree from the Massachusetts Institute of Technology (MIT), Cambridge, in 1997.

He is an Associate Professor and the Holder of the Dietz Career Development Professorship II in the Department of Mechanical Engineering, Texas A&M University (TAMU), College Station. He holds three U.S. patents on precision positioning systems.

Prof. Kim was the recipient of the NASA Space Act Award in 2002, the 2005 Professional Engineering Publishing Award for the best paper published in 2004 in *Journal of Engineering Manufacture*, and the BP Teaching Excellence Award by TAMU College of Engineering in 2006. He is Technical Editor of IEEE/ASME TRANSACTIONS ON MECHATRONICS, *ASME Journal of Dynamic Systems, Measurement and Control*, and *International Journal of Control, Automation, and Systems*.